RSC Advances

PAPER

Cite this: *RSC Adv.*, 2014, **4**, 53575

Factors driving the self-assembly of water-soluble calix[4]arene and gemini guests: a combined solution, computational and solid-state study†

Carmela Bonaccorso,*[a] Giovanna Brancatelli,[b] Giuseppe Forte,[c] Giuseppe Arena,[a] Silvano Geremia,[b] Domenico Sciotto[a] and Carmelo Sgarlata*[ad]

Received 27th August 2014
Accepted 9th October 2014

DOI: 10.1039/c4ra09353d

www.rsc.org/advances

Negatively charged gemini guests in the presence of a tetracationic host trigger the formation of self-assembling structures at physiological pH in water generating entities of the HG and H_2G type (H = host and G = guest). ITC measurements show that the gemini guests are included *via* concerted electrostatic and hydrophobic interactions and that the formation of the HG adduct is enthalpically driven while the formation of the capsular entity (H_2G) is driven by entropy gain. It is shown that the efficiency of capsule formation is influenced by the number of $-CH_2-$ units contained in the spacer and that spacers with an even number of methylene groups seem to be the best templating agents. In line with the above picture, MD simulations and DFT calculations show that the entropic contribution strongly depends on the length of the polymethylenic spacer. In the solid state, for the HG assembly three different structures are revealed by single crystal X-ray diffraction; the flexible interacting units create multiple interactions reaching the optimum balance between inter- and intramolecular energies. To the best of our knowledge, these are the first structures ever reported for water-soluble calixarenes and organic anions.

Introduction

Non-covalent, weak interactions are major tools used in supramolecular chemistry to manage molecular recognition and self-assembly phenomena for the design and synthesis of a variety of novel and intriguing structures such as molecular capsules, cages, flasks and clefts.[1–5] By mimicking the active sites and pockets of enzymes, synthetic capsular assemblies are able to reversibly isolate suitable guest molecules from the surrounding media and promote chemical reactions with other partners in a controlled fashion or stabilize reactive intermediates.[6,7] Confined molecules behave differently than those in free solution[8] and reversible encapsulation processes have been recently used as an effective strategy to isolate molecules in small spaces which could act as containers for the development of unusual reaction pathways[9] or the stabilization[10] and transport of biologically relevant compounds.[11]

Among potential target guests, anions have received great attention from a broad range of researchers; their selective recognition has encouraged applications in a variety of areas of science and technology.[12–14] Anions play many vital roles in biological systems[15] for the preservation of life but may also have harmful effects on the environment as pollutants.[16] Consequently, in the last decades, several synthetic systems, often containing specific functionalities on appropriate platforms/scaffolds,[17] have been elegantly designed and employed for anion recognition/sensing. In this context, the use of constrained systems able to generate a discrete microenvironment that isolates the guest from the bulk of the solvent may help satisfying the coordination features (variety of shapes and geometries, large solvation energies, *etc.*) of demanding species such as anions.[18] The development of supramolecular architectures assisted/triggered by anionic compounds has been widely reviewed,[19] though not many examples have been reported on the recognition of these charged species in water.[20]

Supramolecular chemistry is nowadays smartly moving towards the aqueous domain in order to involve biochemistry or stimulate new paths in green chemistry related fields.[21,22] The dramatic differences between the bulk water and the inner space within a molecular container[23] provide the "thermodynamic boost" to guest complexation which, in this peculiar solvent, cannot be driven only by structural complementarity or fitting between the host and the guest.[24,25] Such findings were also supported by quantum chemical calculations carried out for modeling the transport of alkali ions through isolated cell

[a]*Dipartimento di Scienze Chimiche, Università degli Studi di Catania, Viale A. Doria 6, 95125, Catania, Italy. E-mail: sgarlata@unict.it; bonaccorsoc@gmail.com*

[b]*Centro di Eccellenza di Biocristallografia, Dipartimento di Scienze Chimiche e Farmaceutiche, Università degli Studi di Trieste, Via L. Giorgieri 1, 34127, Trieste, Italy*

[c]*Dipartimento di Scienze del Farmaco, Università degli Studi di Catania, Viale A. Doria 6, 95125, Catania, Italy*

[d]*Consorzio I.N.B.B., Viale delle Medaglie d'Oro 305, 00136, Roma, Italy*

† Electronic supplementary information (ESI) available. CCDC 1002190, 1002197, 1002465 and 1005754. For ESI and crystallographic data in CIF or other electronic format see DOI: 10.1039/c4ra09353d

membrane ion channels.[26] Consequently, unveiling the thermodynamic and structural parameters and forces that are at the base of anion-templated assemblies in water is a key point for the rational design of efficient capsular containers for anions.

Within this framework, we have recently shown that a tetracationic calix[4]arene receptor (**TAC4**, Scheme 1) is able to recognize organic anions with different functionalities, shapes, charge[27,28] and to form supramolecular capsules in water at physiological pH.[29] Specifically designed guests, having two aromatic and negatively charged head groups (**BSCn**, $n = 2$ and 6, Scheme 1), trigger the self-assembling of homodimeric capsules with **TAC4** relying on concerted hydrophobic and electrostatic interactions.[30] Capsule formation in water has been undoubtedly confirmed by a host of techniques such as combined NMR, MS and ITC data. The above gemini guests interact with the calixarene by inserting their aromatic moieties into the lipophilic pocket of the host while placing their polar sulphonate groups at the charged upper rim of the calixarene.

With the aim of investigating whether and to what extent spacers having different length would still permit capsule templation, a series of guests with variable $-(CH_2)_n-$ linkers ($n = 2$–6) have been synthesized and their interaction with **TAC4** preliminary screened *via* NMR.[31] The results suggested that additional relevant factors, such as guest size and shape, may deeply affect the assembly process.

Here we report on a detailed nano-calorimetric (ITC) investigation of a series of **BSCn–TAC4** systems in neutral aqueous solution; the length of the guest spacer has been varied to single out the forces driving the formation of the host–guest complexes and hence to envision the best strategy for the construction of effective capsular structures. The ITC analysis has been coupled with molecular dynamics (MD) and DFT calculations which provide further information on the thermodynamics of complexation and hints on the capsule templation process. The host–guest systems have been also investigated in the solid-state; X-ray crystal structures have been obtained for both **TAC4** and its complexes with **BSC2**. On the whole, results from both solution and solid state provide relevant insights into the molecular recognition process in terms of structure/conformation of the components as well as distances among guests and host functional groups.

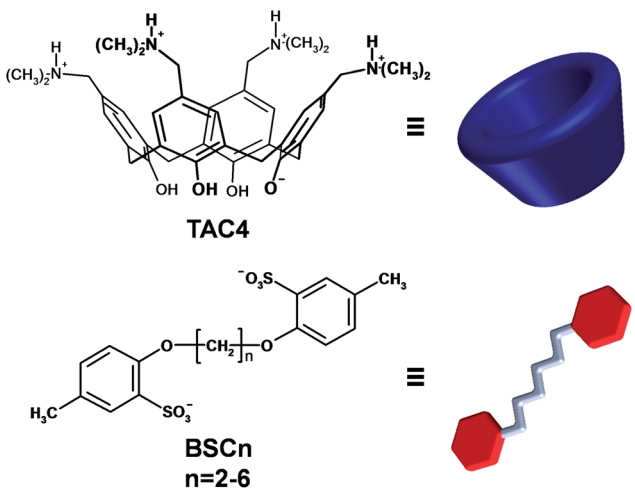

Scheme 1 Schematic of the host (TAC4) and the guests (BSCn) investigated.

Results and discussion

TAC4–BSCn host–guest complexes were originally investigated *via* ^{1}H NMR titrations which showed that the dianionic guests are included through their aromatic moiety with the methyl groups pointing into the host cavity. The refinement of the NMR data allowed for the determination of the 1 : 1 and 2 : 1 host–guest binding constants.[29–31] Previous diffusion NMR (DOSY) experiments revealed that, in the presence of increasing amounts of **TAC4**, guests diffuse more slowly than in their free form as a consequence of their larger size resulting from complex formation. DOSY data could be satisfactorily fit only when both HG and H_2G (H = host, G = guest) complexes are formed in solution.[31] Furthermore, 2D ROESY NMR spectra indicated that **TAC4** hosts are wrapped around the guest ends.[29,30] The free energy of binding determined through NMR experiments was double checked by isothermal titration calorimetry (ITC); ITC was also employed to determine the energetics of the inclusion and self-assembly processes in solution.[32,33]

The driving forces for the capsule formation include specific, non-specific, weak interactions[34,35] between the gemini guests and the host as well as contributions resulting from the desolvation of the host and the guest; noteworthy, these factors may have different and often opposing enthalpic and entropic contributions[36,37] and thus splitting the free energy term into the ΔH° and ΔS° components may help understanding capsule formation equilibria and reveal specific features and differences among the various **BSCn** guests that are not expressed in the ΔG° term.

Calorimetric experiments were carried out in buffered aqueous solution (pH 6.8) to minimize any contribution resulting from the interaction of either **TAC4** or **BSCn** with the proton. A typical thermogram for the **BSC4–TAC4** system at 25 °C is shown in Fig. 1 (further ITC titration data are reported in the ESI†). Due to the procedure used for the ITC titrations (increasing amounts of the guest are added to the host), the equilibrium between the 1 : 1 (host–guest) and 2 : 1 (capsule) complexes is shifted towards the capsule formation in the presence of excess host, that is, in the first region of the curve only.[29,30] This implies that a relatively large number of titration points had to be collected to obtain an accurate fit of the whole curve.

The thermodynamic parameters for the interaction of different **BSCn** guests with **TAC4**, determined by using a software which refines data from multiple titrations, are reported in Table 1. These data reproduce the speciation and the binding constants trend obtained *via* ^{1}H NMR, provided due allowance is made for the different experimental procedures and conditions employed.[31] Both techniques indicate that the HG and the H_2G complexes coexist in solution at neutral pH. Different species and combinations thereof were examined but the data

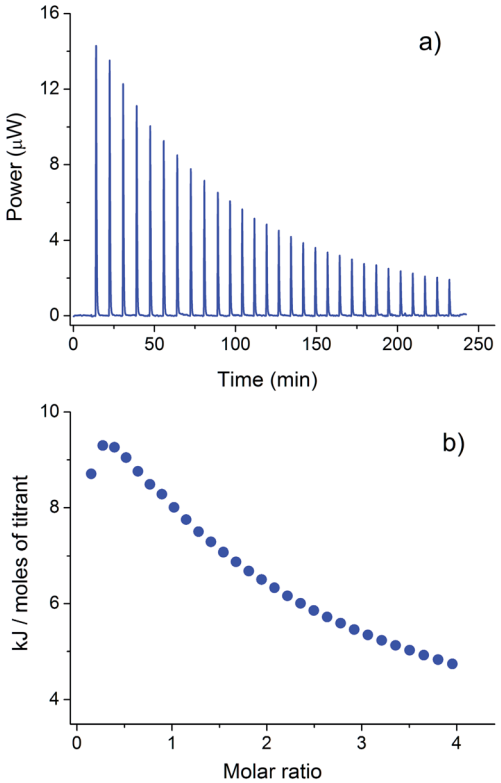

Fig. 1 (a) Typical ITC titration of **BSC4** into **TAC4** in buffered aqueous solution (pH 6.8) at 25 °C and (b) integrated heat data.

analysis invariably converged to the species and values reported in Table 1.

The plot of the log *K* values for the HG and H_2G species as a function of the CH_2 groups on the guest spacer evidences interesting differences for the binding regarding the two species (Fig. 2).

Log K_1 values are similar to each other regardless of the number of CH_2 units on the linker of the various **BSCn**; the inclusion process that leads to the formation of the HG species appears to be somehow unaffected by the length of the alkyl

Table 1 Thermodynamic parameters[a] for the host–guest complex (HG) and the capsule (H_2G) formation at 25 °C in buffered aqueous solution (pH 6.8)

Guest	Species	Log *K*	$\Delta H°$ (kJ mol^{-1})	$\Delta S°$ (J deg^{-1} mol^{-1})
BSC2	HG	3.63(8)	−23.75(8)	−10(2)
	H_2G	3.4(4)	15.4(1)	117(8)
BSC3	HG	3.58(2)	−19.95(7)	1.6(4)
	H_2G	2.30(3)	10.4(4)	79(2)
BSC4	HG	3.45(9)	−22.7(1)	−10(2)
	H_2G	3.1(4)	14.7(5)	109(8)
BSC5	HG	3.38(3)	−19.0(1)	1.0(7)
	H_2G	2.55(4)	13.6(7)	95(3)
BSC6	HG	3.46(3)	−19.21(6)	1.8(6)
	H_2G	2.9(3)	13.3(2)	100(4)

[a] σ in parentheses.

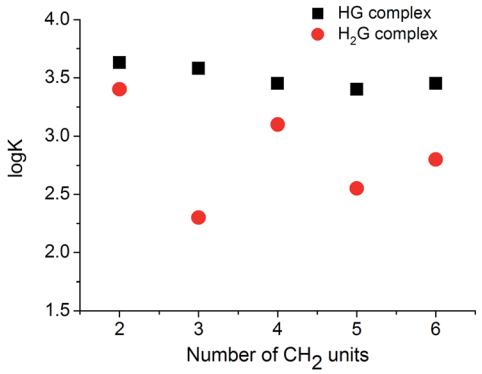

Fig. 2 Plot of the log *K* values as a function of the number of methylene groups on the guest spacer.

chain of the guest. This sounds reasonable as, to form the 1 : 1 complex, the upper rim and the cavity walls of the host interact only with one of the two aromatic and negatively charged ends of the gemini guest (as would interact a simple mono anionic molecule) and, thus, the inclusion process does not depend on the dimension/size of the guest. Conversely, log K_2 values indicate that **BSCn** having $n = 2, 4, 6$ form supramolecular capsules with comparable stability while guests having $n = 3, 5$ assemble into less effective capsular entity, as previously observed through ^{1}H NMR data.[31] The molecule with the shorter spacer, **BSC2**, is able to trigger the formation of the most stable capsule (log $\beta_2 = 7.03$) probably as it enables a tighter connection of the guest between the two facing calixarenes.[30] On the whole, the efficiency of the capsule templation process seems to be markedly affected by the different length and number of methylene units on the alkyl chain of the guests.[38] As shown in Fig. 2, the ability of the different **BSCn** guests to form supramolecular capsules proceeds in keeping with an "even-odd" fashion and the stability of the assemblies formed with guests having an even number of CH_2 slightly decreases as the size of the spacer increases. Shape and dimensions along with conformational and steric features of the linkers of the various **BSCn** strongly influence the arrangement and the binding of the two hosts during the encapsulation process of the double-headed guests in solution. This peculiar "odd-even" alternation effect has been observed for long time now in other processes such as nucleophilic displacement reactions of some homologous series of alkyl derivatives[39] and the formation of a series of fluoranil–alkylbenzene complexes.[40] Effects depending on the relative orientation of the functional groups to the carbon atom at which the specific reaction occurred were thought to contribute to the alternation in either the rate or the association constant. Odd-even trends were also reported for processes involving, among others, ionic liquids,[41] polysaccharide-surfactant systems,[42] self-assembled monolayers,[43] alcohols[44] as well as the melting point of normal carboxylic acids.[45]

The enthalpic and entropic contribution to the free energy term are shown in Fig. 3. The figure gives an immediate perception of the differences between the simple inclusion of

one polar head only and the capsule formation (*i.e.* between the HG and H_2G species). We have to point out that the values determined earlier on for the **BSC6–TAC4** assembly[29] seemed to be an outlier when compared with those of the entire series reported here. This prompted a reinvestigation of the first system ever reported by our group (*i.e.* the **BSC6–TAC4** system) under the same conditions employed for the study of all the terms of the series. In the reinvestigation, the precision and accuracy of the calorimetric apparatus was thoroughly tested by using the chemical calibration procedure previously described in details[46] rather than simply resorting to an electrical calibration. The latter procedure, although recommended by ITC manufacturers, can be subject to significant error especially because of a different distribution of heat from the calibration heater than from a chemical process.[47,48]

The complexation of the guests by **TAC4** to form the 1 : 1 species is both enthalpically driven and favored regardless of the size of the **BSCn** (Fig. 3a). Electrostatic interactions between the sulfonate groups of the guests and the positively charged upper rim of the host, along with CH–π and π–π interactions with the **TAC4** cavity, drive the host–guest complex formation. These enthalpically favorable contributions override the cost in energy needed for the desolvation of all the interacting reagents. The entropic contribution to ΔG° for each **BSCn** is the result of the fine balance between host and guest desolvation ($\Delta S^\circ > 0$) and the loss of degrees of freedom due to HG complex formation ($\Delta S^\circ < 0$).

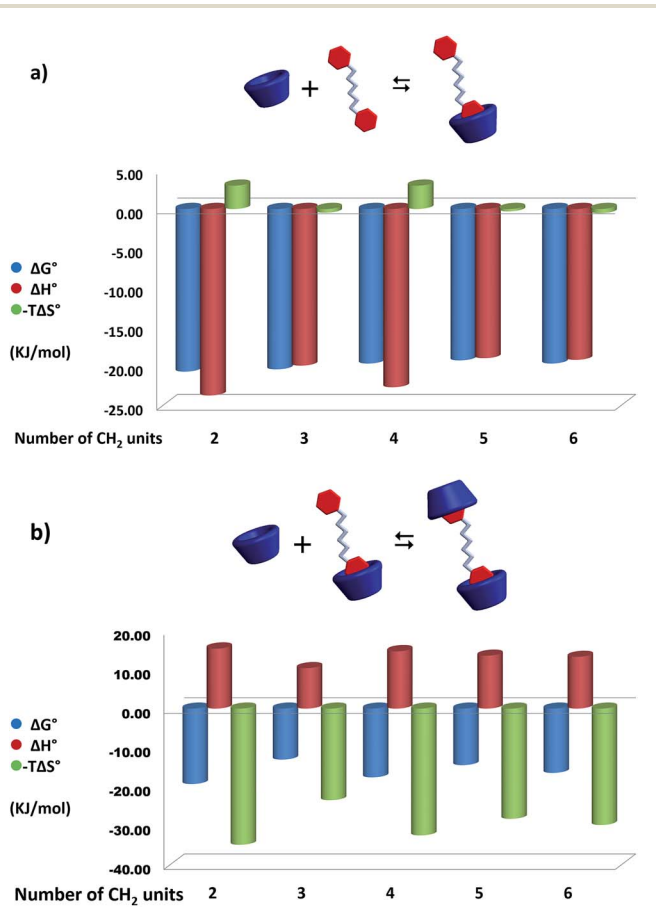

Fig. 3 Thermodynamic parameters for the host–guest complex (a) and capsule formation equilibria (b) at 25 °C in water (pH 6.8).

The capsule assembling discloses a totally different picture (Fig. 3b). In all cases, the reaction is entropically driven[49] and enthalpically unfavored: the desolvation needed for the incorporation of the guest molecules into the host cavity is the driving force of the process[50] and overrides the entropic penalty associated with organizing the dianion and the receptors into a more complex architecture. Interestingly, $T\Delta S^\circ$ values mirror the "odd-even" trend seen for the free energy term thus highlighting the key role played by the entropy in the formation of the capsular structure. Capsules triggered by even-numbered guests are more stable and show larger ΔS° values (which regularly decrease as n increases); less stable assemblies (with $n = 3, 5$) are characterized by smaller entropic contributions. Positive values of ΔH° found for all the 2 : 1 systems indicate that the enthalpic cost for desolvation and the Coulombic repulsion between the positively charged hosts that face each other in the capsule prevail over the attractive (ionic and hydrophobic) interactions which allows for the burying of the aromatic moieties of the guest into the host cavity.

Interestingly, most of these competing/balancing contributions (such as steric hindrance, electrostatic repulsion, guest rigidity, *etc.*) tend to level out as the length of the alkylic linker increases. Indeed, Table 1 and Fig. 3 show that ΔH° and ΔS° for **BSC5** and **BSC6**, *i.e.* the longest spacers, are quite similar for both the HG and the H_2G species.

In order to have additional details on the formation of the capsular assembly and to shed further light on the factors determining the odd-even effect detected for its formation we carried out an MD and DFT study. As described above, NMR data[29–31] indicate that in the HG complex the methyl group of one gemini end of the guest is inserted into the calixarene cavity while the neighboring sulphonate residue is located on the upper rim by virtue of its interaction with the positively charged ammonium groups decorating the upper rim of the calixarene. Accordingly, the arrangement shown in Fig. 4a was set as the starting model for the MD calculation; in this figure water molecules are not reported for the sake of clarity. Since each benzene unit of the guest contains a methyl carbon and a sulfur atom that may or may not be included in the cavity, henceforth we will use the subscript i and e to denote atoms that are located within or outside the cavity, respectively. Analogously, for the host the subscripts c and f will be used to indicate complexed and free host, respectively.

For the HG type of complexes, the structures selected by means of molecular dynamics (MD) were further relaxed in DFT; energy minima show that, except for the case of **BSC2**, the guest is folded regardless of the length of the polymethylenic spacer.[51] Indeed, stability is due to an electrostatic contribution (involving both ion–ion and ion–dipole interactions) and van der Waals short-range forces. Electrostatic attraction between negative S_e and positive quaternary ammonium groups determines the folded arrangement shown in Fig. 4b. The computed energy values show that $-(CH_2)_2-$ is the spacer which minimizes the repulsive contributions and maximizes the attractive

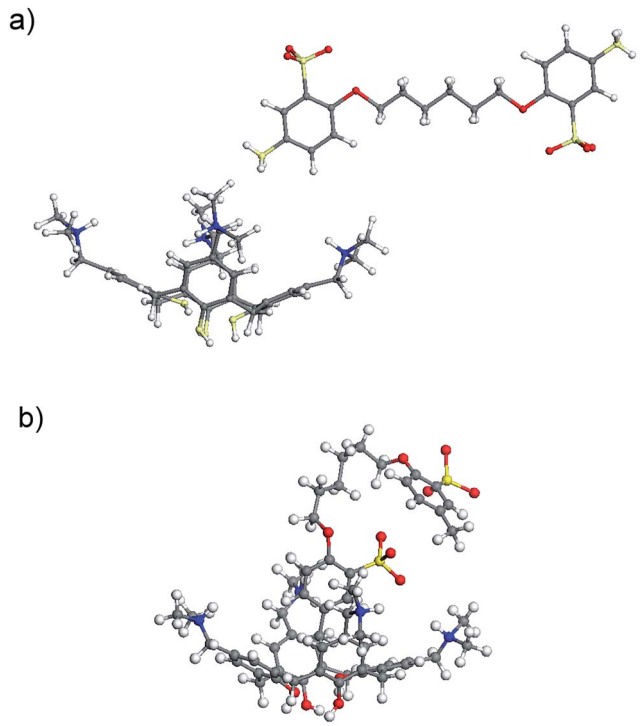

Fig. 4 (a) Starting model of the HG complexes. (b) Folded structure obtained after optimization. TAC4–BSC6 system is reported as an example.

interactions. Computed binding energies, in terms of enthalpic contributions, turned out to be 27.51, 22.64, 25.45, 23.28 and 19.32 kJ mol^{-1} for $n = 2$, 3, 4, 5 and 6, respectively. Such values are in good agreement with the experimental data obtained *via* ITC, provided due allowance is made for the slight energy differences among the various **BSCn–TAC4** systems and the limitations inherent in the computational method.

The flexibility (see below) of the spacer is at the basis of the interaction with an additional host$_f$ molecule. This parameter, that predominates over all the interaction forces, was studied in terms of variation of the distances between S_e and the closer nitrogen atom of the ammonium quaternary groups during MD; fluctuations of the distance S_e–S_i and C_e–C_i of the guests were also analyzed (Fig. 5).

The analysis emphasizes a considerable increase of the distances for longer spacers, if compared to the –$(CH_2)_3$– linker, during the time evolution. Due to the lack of flexibility, the analyzed distances in the case of the –$(CH_2)_2$– spacer are comparable, or even higher, than those of the longest methylene chain (**BSC6**). Fig. 5 clearly indicates the fluctuation of the negative aromatic moiety external to the host (*i.e.*, not involved in the complexation) and may explain, from a kinetic point of view, the inclusion of the second polar head of the pre-existing HG species into an additional host$_f$ moiety. Remarkably, longer distances were detected for $n = 2$, 4 and 6; it follows that the free negative guest moiety exerts, through the solvent, a stronger attractive force towards the positively charged hosts$_f$ and, on the other hand, the slighter steric hindrance due to the longer distance from host$_i$ allows for a deeper inclusion of the free end of the guest into host$_f$.

In the host–guest interaction both kinetic and thermodynamic perspective should be considered. The initial events are ruled by kinetics as the free negative moiety of the guest, *i.e.* the external sulphonate group, experiences the long range attractive forces due to the positive ammonium groups of the hosts$_f$. This

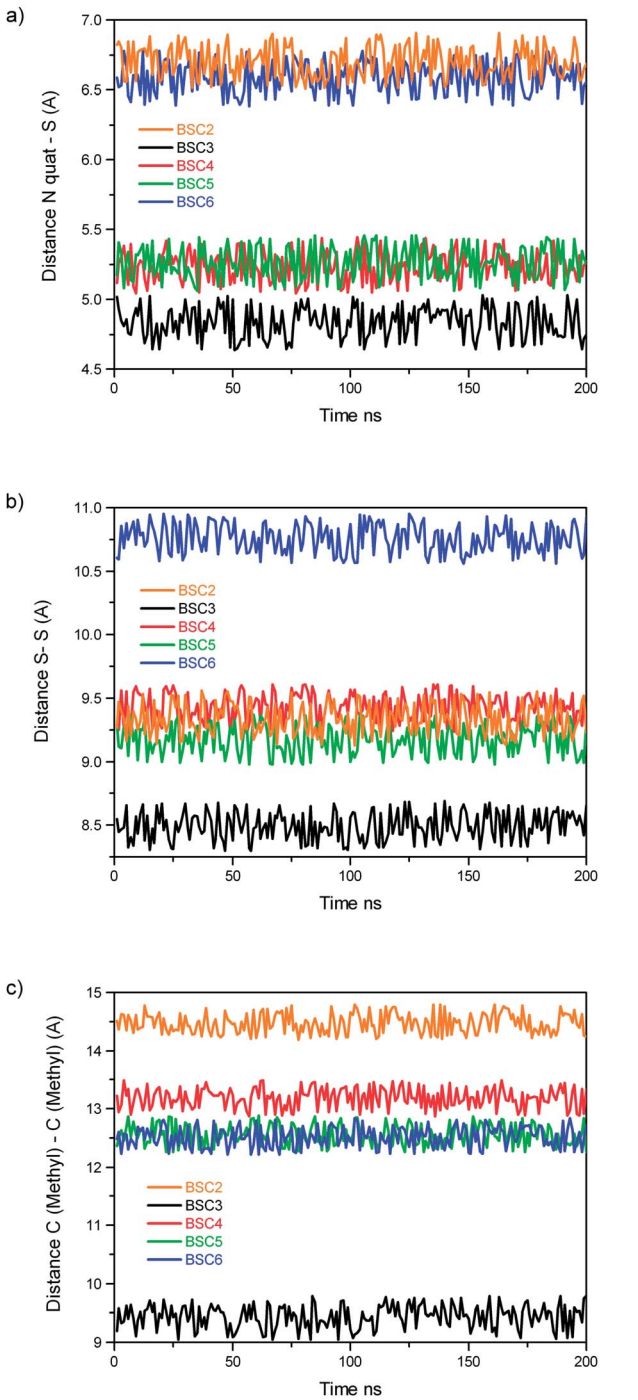

Fig. 5 Time evolution of the distances between sulphur–quaternary nitrogen atom (a), included and external sulphur atom (b) and included and external carbon atoms of the methyl groups (c).

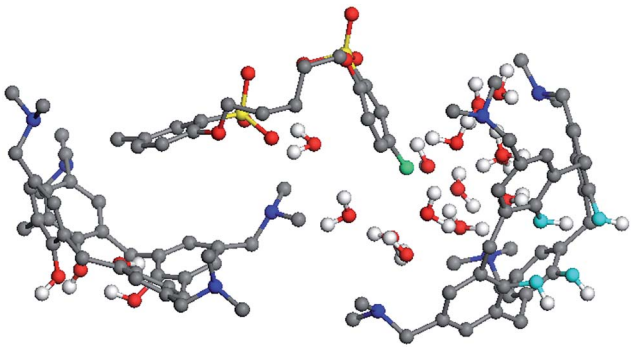

Fig. 6 Model for the encapsulation of a guest into a second host molecule. For the sake of clarity, hydrogen atoms are shown only in the water molecules reported (in red) and in the H-bond chain at the lower rim of the calixarenes (in cyan). The external methyl carbon C_e is displayed in green.

event is followed by a thermodynamic rearrangement of the structure leading to the insertion of C_e and the largest part of the aromatic ring inside the cavity of the $host_f$, as shown by NMR data.[31]

Calorimetric results indicate that the formation of the H_2G capsular adduct is driven by the favorable entropic contribution due to increasing solvent disorder which, in turn, results from to the desolvation of the calixarene cavity. This prompted a study of the desolvation process in MD by simulating the insertion of C_e into the $host_f$ and, at the same time, the removal of $host_f$ physisorbed water molecules. Starting from MD results obtained for the 1 : 1 complexes simulations, $host_f$ was "placed" in such a way as to promote the encapsulation of the guest (Fig. 6).

During the time evolution, the fluctuation of the average distance among oxygen atoms of the water molecules physisorbed within the $host_f$ cavity, O_w, and atoms involved in the hydrogen-bond chain at the lower rim of the $host_f$, O_b, was analyzed (Fig. S1†). Fluctuations of the average distance between C_e and O_b were also examined (Fig. S2†). The analysis points out that the longest O_w–O_b distance was found for the guest with the $-(CH_2)_2-$ spacer which, as a consequence, is better included into the $host_f$ cavity, as also suggested by the shortest C_e–O_b distance calculated for **BSC2**. A similar trend was observed for the **BSC4** and **BSC6** guest. Conversely, a partial/incomplete inclusion was found for $n = 3$ and 5; the insertion is somehow hindered by the steric hindrance due to the close distance $host_c$–$host_f$ and the desolvation process is less pronounced for $n = 3$. Incidentally, this was to some extent observed also for $n = 5$ as shown in Fig. S2.† Taken all together, the above results lead to the conclusion that the entropic contribution strongly depends on the length of the polymethylenic spacer and decreases by following the order $n = 2$, 4, 6, 5, 3.

The **TAC4–BSCn** systems were also explored in the solid-state. Contrary to the most commonly explored sulfonate calixarenes, very few crystal structures of calix[4]arenes with cationic organic moieties at the upper rim have been reported so far[52] and even fewer examples have been reported for water soluble systems;[53] moreover, to the best of our knowledge, no host–guest complex formed by a water-soluble cationic calixarene and an organic anion has ever been described in the solid state.

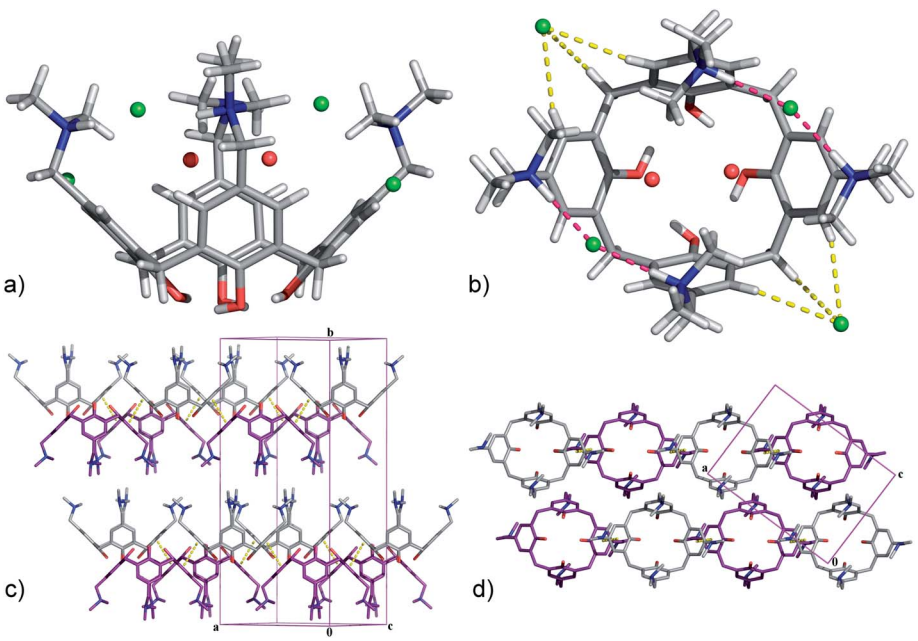

Fig. 7 Crystal structure of calixarene **TAC4**: side (a) and top (b) view; external water molecules were omitted for clarity, dashed magenta and yellow lines represent the intermolecular N–H···Cl and C–H···Cl interactions between the receptor and the chloride anions. Crystal packing of **TAC4**: side (c) and top (d) view; π···π stacking interactions connect adjacent host molecules with opposite orientation, leading to the formation of a double layer.

The crystal structure of **TAC4** obtained by X-ray analysis (see Experimental section and Table S1†) is shown in Fig. 7. The asymmetric unit consists of half receptor molecule, two chloride anions and 2.5 water molecules. The two halves of the receptor are symmetry-related by a crystallographic two-fold axis perpendicular to the mean plane defined by the four methylene bridging groups of the calixarene; thus the **TAC4** host adopts a C_{2v}-symmetry conformation with dihedral angles between the aromatic rings and the methylene mean plane of 114.0(1) and 134.8(1)°. This is in line with findings based on *ab initio* calculations.[54] The dimethylammonium groups lock one chloride anion through two hydrogen bonds (N···Cl 3.065(5) and 3.087(5) Å), whereas the second chloride anion interacts with the calixarene external walls through C–H···Cl interactions (2.861–3.181 Å). The aromatic cavity is filled by two water molecules at partial occupancy.

The calixarene aromatic rings are involved in π···π stacking interactions with the neighboring host molecules (the distance between the centroid of the facial aromatic rings is 3.46(1) Å) and the layers are arranged so that the top rims bearing the ammonium groups point toward each other (Fig. 7c and d). This up-down antiparallel bilayer arrangement creates both hydrophobic and hydrophilic environments and mimics structure and properties of naturally occurring clays, as previously reported for analogous *p*-sulfonatocalix[4]arene.[55]

Single-crystal X-ray diffraction analysis reveals the formation of inclusion complexes of **TAC4–BSC2** having a 1 : 1

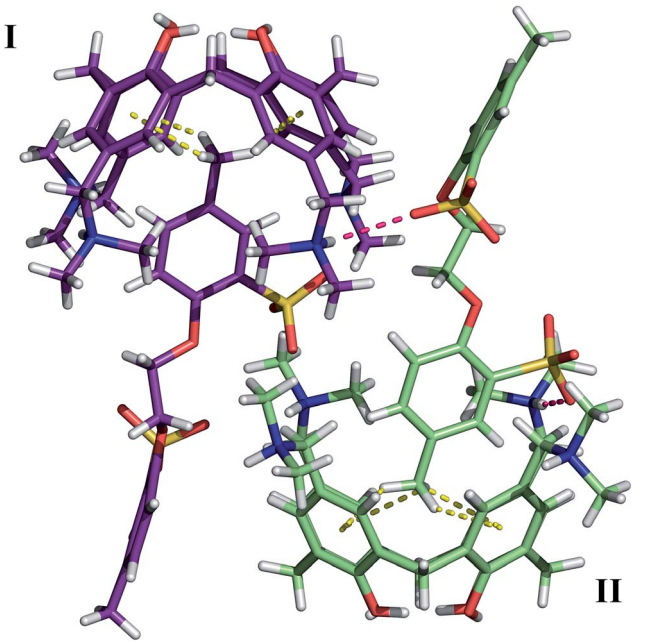

Fig. 9 Solid state structure of the inclusion complex **2**. The two crystallographic independent host–guest complexes, labelled I and II, were depicted in violet and green, respectively. Dashed magenta and yellow lines represent the intermolecular hydrogen bonding and C–H···π interactions between host and guest. Chloride anion and water molecules were omitted for clarity.

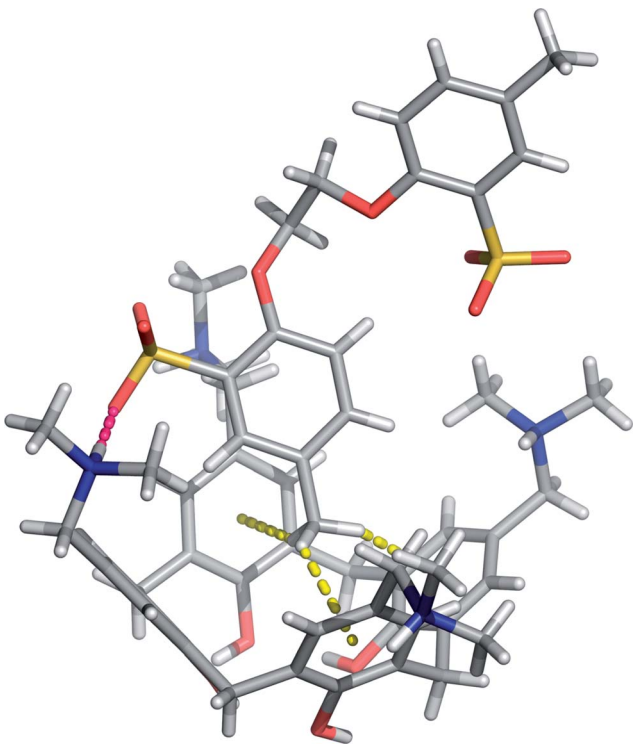

Fig. 8 Solid state structure of the inclusion complex **1**. Dashed magenta and yellow lines represent the intermolecular hydrogen bonding and C–H···π interactions. External counterions (**BSC2** and chloride) and water molecules were omitted for clarity.

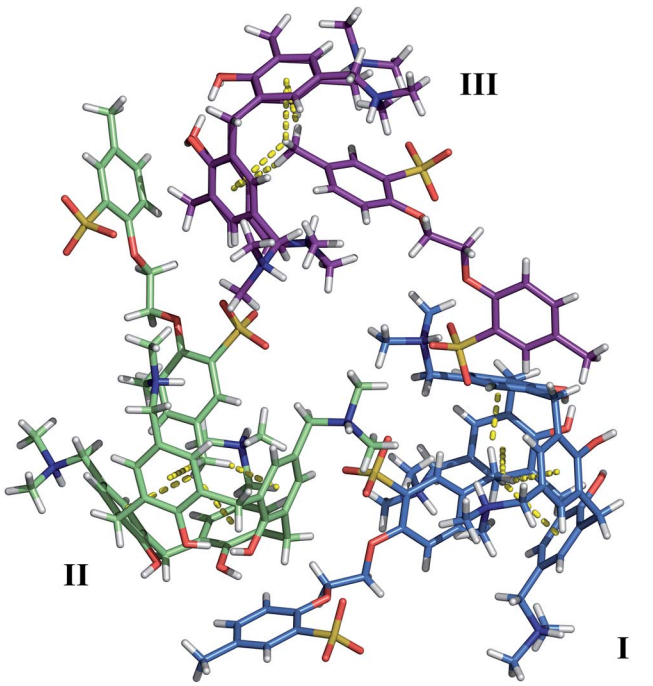

Fig. 10 Solid state structure of the inclusion complex **3**. The three crystallographically independent host–guest complexes were labelled I, II and III. Dashed yellow lines represent the intermolecular C–H···π interactions between host and guest. Chloride anion and water molecules were omitted for clarity.

stoichiometry (see crystals **1**, **2** and **3** in Fig. 8–10, respectively). In the triclinic crystal **1** the asymmetric unit contains one biscationic **BSC2–TAC4** complex, one chloride anion and half centrosymmetric **BSC2** bisanionic molecule acting as counterion (Fig. S3 and S4†). Two crystallographically independent **BSC2–TAC4** complexes (designated hereafter as I and II) are electrically balanced by four chloride anions for the triclinic form **2** (Fig. S5 and S6†), while three crystallographically independent **BSC2–TAC4** complexes (designated hereafter as I, II and III) and six chloride anions are present in the asymmetric unit of the trigonal form **3** (Fig. S7†).

Crystals **1**, **2** and **3** are examples of *endo*-complexation between **TAC4** and **BSC2**, nevertheless, they significantly differ as concerns the guest conformation as well as the overall crystal packing arrangement. In each complex the methyl group of one end of the **BSC2** guest is located within the calixarene cavity, whereas the other end protrudes outside the cavity. The attraction between the guest methyl group and the calixarene aromatic walls is driven by C–H$\cdots\pi$ interactions (distances are listed in Table S2†). In addition, the complex **1** and one crystallographic independent complex in **2** (II) show a direct hydrogen bond between the positively charged dimethylammonium fragment and the negative sulfonate group, contributing to the overall complex stabilization (N$\cdots$O 2.71(2) Å in **1** and 2.79(2) Å in **2**, Fig. 8 and 9).

In crystal **1** the **TAC4** host adopts a pseudo-C_{2v}-symmetry conformation with almost equal dihedral angle values between opposite aromatic rings and the methylene mean plane. By contrast, in crystals **2** and **3** the receptor cavity adopts a pseudo-C_{4v} cone conformation, except for a slight distortion in the complex I of crystal **2**. In **1** and **2** the aromatic *endo*-plane of **BSC2** is slantwise oriented with respect to the calixarene mean plane with dihedral angles of 68.3(1)° in **1** and 69.2(1), 69.4(1)° in **2**, whereas the guest is almost orthogonal in the case of **3**, showing dihedral angles ranging from 82.06(2) to 88.47(2)° (see Table S3†).

In complex **1**, the *exo*-coordinated end of **BSC2** is folded towards the upper calixarene, whereas in the crystal structures **2** and **3** the guest exhibits a more extended conformation, with the two aromatic planes rotated by approximately 90°, around the O–CH_2–CH_2–O fragment (Fig. 9 and 10). Despite the different guest conformation, in all the three structures the

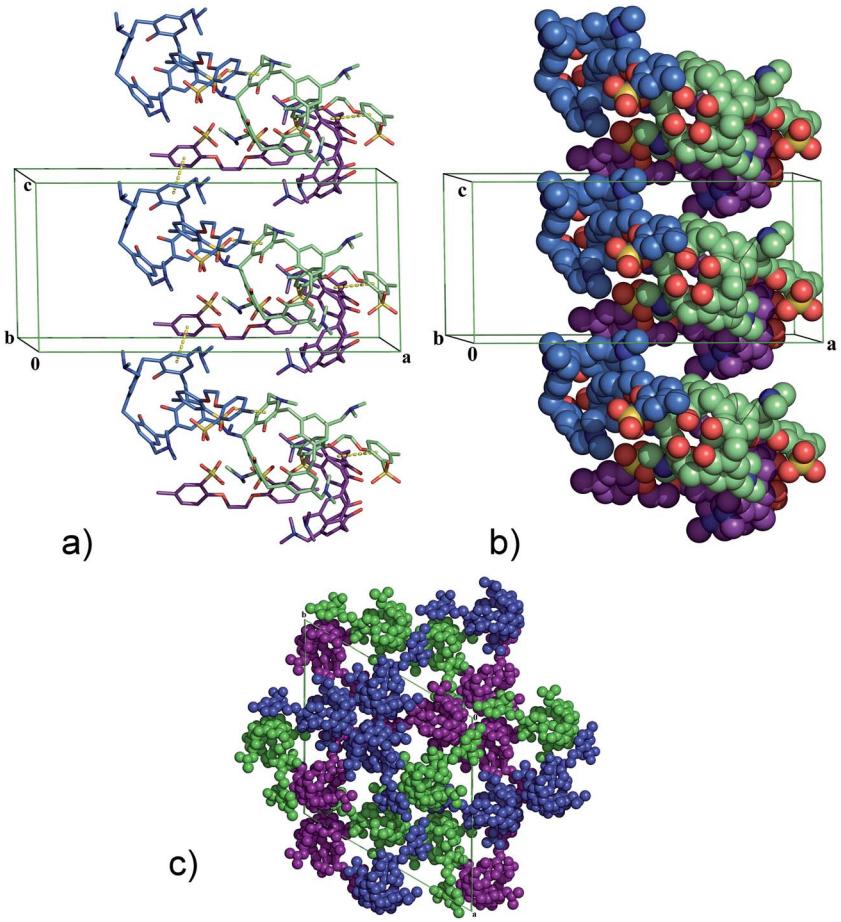

Fig. 11 (a) Detail of $\pi\cdots\pi$ stacking interactions between the *exo*-end of **BSC2** guest and the aromatic ring of adjacent **TAC4** molecule (distances range between the centroid of the aromatic rings is 4.22–4.29 Å). (b) Helical one-dimensional chain of the trimeric assembly along the crystallographic *c* axis by virtue of three $\pi\cdots\pi$ stacking interactions. (c) View of the molecular packing along the *ab* plane, showing the cavities filled by solvent molecules and chloride anions. Water molecules and chloride anions were omitted for clarity.

exposed end of **BSC2** is engaged in multiple non-covalent interactions (H-bonds, C–H···π and π···π stacking interactions), driving the various molecular packing arrangements observed for the three complexes.

In crystal **1** the *exo*-sulfonate group of **BSC2** is hydrogen bonded to a water molecule (O···O 2.82(2) Å), while also forming weak hydrogen bonds with two surrounding methyl groups from cationic fragments (C···O 3.47(1) and 3.24(1) Å); the aromatic ring is involved in C–H···π interactions (C···Cg 3.55(5) Å, where Cg is the centroid of the aromatic ring) with a neighboring calixarene molecule (see Fig. S3†). By virtue of such an arrangement, chains of alternated 1 : 1 complexes form along the crystallographic *bc* plane (see Fig. S4†).

In both crystals **2** and **3** there are several water molecules solvating the anionic *exo*-sulfonate moieties (O···O 2.71–2.88(2) Å in **2** and O···O Å 2.78–2.86(8) in **3**, respectively), leading to the formation of dense hydrogen bonding networks that contribute to the overall stabilization of the **BSC2–TAC4** complexes (Fig. S5 and S7†). In addition, in **2** both exposed aromatic rings of **BSC2** are involved in C–H···π interactions with the methylene group at the upper rim of a neighboring cationic calixarene (C···Cg 3.84–3.94(5) Å). On the contrary, in structure **3** the *exo*-ends of **BSC2** guests are involved in π···π stacking interactions with the aromatic rings of the adjacent **TAC4** molecule (Fig. 11a) (Cg···Cg 4.22–4.29(8) Å). These interactions drive the structural arrangement of the trimeric unit in a left-hand helical chain along the *c* axis (Fig. 11b) leading to the formation of cavities filled by clathrated chloride anions and water molecules along the *ab* plane (Fig. 11c).

Very recent results elegantly emphasize that in flexible structures the molecular geometry may be distorted under the influence of intermolecular interactions in a crystal structure to reach the optimum balance between inter- and intramolecular energies.[56] Hence, the geometries detected in the solid state may differ from those observed in solution due to the requirements of the close-packed environment in a crystal structure. In our systems, thanks to the flexibility of the interacting units, multiple interactions occur between the guest and the neighboring hosts as well as between the guests and the hosts, water molecules and counter ions which ultimately lead to more easily crystallizing neutral structures.

Conclusions

Negatively charged gemini guests with spacers of different length may be successfully employed as templating units to obtain self-assembled capsular entities in the presence of a tetracationic host in water at physiological pH. ITC measurements show that anion recognition leading to the formation of the HG adduct is enthalpically driven and **BSCn** are included *via* concerted electrostatic and hydrophobic interactions. Conversely, capsule formation is a process that is driven by entropy gain due to the release of water molecules from host and guest upon encapsulation. The number of $-CH_2-$ units of the alkyl chain of the guest affects the efficiency of the capsule formation; molecules with a spacer having an even number of methylene groups seem to be the best templating agents.

MD simulations and DFT calculations support the view that the formation of the HG complexes is enthalpically driven regardless of the value of "*n*" and the formation of the capsular assembly is determined by the entropic contribution (mostly due to desolvation) and strongly depends on the value of "*n*". Factors such as steric hindrance and the choice of proper distances among relevant functional groups of both host and guest turn out to be crucial for the appropriate and efficient construction and self-assembling of the supramolecular entity.

Single crystal X-ray diffraction reveals the formation of **TAC4**/**BSC2** 1 : 1 complexes only. In each complex one end of the gemini guest is inserted into the calixarene cavity, by virtue of C–H···π interactions and hydrogen bonds. On the other hand, in all structures the exposed end of **BSC2** is solvated by several water molecules and, at the same time, is involved in C–H···π or π···π stacking interactions with neighbouring calixarene molecules.

The above findings may be useful for the design and development of anion-templated containers that might serve as nanoscale reaction chambers or shuttles for the confinement and delivery of biological substrates in a demanding solvent such as water.

Experimental

Materials

The host, **TAC4**, was synthesized according to the procedure described by Gutsche *et al.*[57] while the guests **BSCn** (n = 2–6) were obtained as previously reported by our group.[29–31] As the accurate determination of the thermodynamic parameters requires concentrations to be precisely known, the purity of both **TAC4** and **BSCn** was determined through thermogravimetric analysis (TGA); the purity of **TAC4** was additionally checked by potentiometric titrations, as described previously.[27] Both the host and the guests decompose completely at about 500 °C indicating that they are free from inorganic impurities. The concentrations of **BSCn** and **TAC4** were obtained by correcting for the water amount (8–11%) determined through TGA.

High purity water (Millipore, Milli-Q Element A 10 ultrapure water) and A grade glassware were employed throughout.

ITC titrations

ITC titrations were carried out at 25 °C in water (phosphate buffer, pH 6.8) with a nano-isothermal titration calorimeter Nano-ITC^{2G} (TA) having an "active" cell volume of 0.988 mL and equipped with a 250 or 100 μL injection syringe. Measurements were run in the overfilled mode which does not require any correction for liquid evaporation and/or for the presence of the vapor phase.[58] The power curve was integrated by using NanoAnalyze software (TA) to obtain the gross heat evolved/absorbed in the reaction. The instrument was primarily calibrated chemically by titrating an HCl solution (1 mM) into buffered TRIS (30 mM containing 10 mM HCl so that [TRIS]/[TRISH$^+$] = 2 : 1) following the procedure described previously.[46] Once obtained the calibration factor chemically, the equipment was also checked by

running an electrical calibration. ITC measurements were carried out by titrating an aqueous solution of **BSCn** (0.7–3.5 mM) into a **TAC4** solution (0.3–0.5 mM); both the host and the guests were dissolved in 0.1 M phosphate buffer (pH 6.8). Typically, 8–9 independent experiments were run for each **BSCn–TAC4** system in order to explore both smaller (about 0.25) and larger (up to 3.5) guest/host ratios and thus collect an adequate number of points to obtain a satisfactory fit of both the first and last portion of the curve; the two portions were, however, refined together to obtain the final values. The heats of dilution were determined in separate blank experiments by titrating solutions of **BSCn** (in phosphate buffer) into a solution containing phosphate buffer only. The net heats of reaction, obtained by subtracting the heat evolved/absorbed in the blank experiments, were analyzed by HypΔH.[59] This software is specifically designed for the determination of equilibrium constants and/or formation enthalpies of complexes in solution by non-linear least-squares minimization of the function $U = \sum(Q_{obs} - Q_{calc})^2$. In this function, Q_{obs} is the observed heat for a given reaction step, corrected for the dilution (blank) effects, while Q_{calc} is calculated as $Q_{calc} = -\sum(\delta n \Delta H^\circ)$, where δn is the change, for one reaction step, in the number of moles of a reaction product (calculated in terms of a set of equilibrium constants) and ΔH° is the molar formation enthalpy for the reaction product. The summation is carried out over all the reactions in the system. The squared residuals $(Q_{obs} - Q_{calc})^2$ are summed over all the titration steps. HypΔH also allows for the simultaneous refinement of data from multiple titrations.

Molecular dynamics and DFT calculations

Molecular dynamic (MD) simulations were firstly carried out on the HG adduct with a number of water molecules ranging from 285 ($n = 2$) to 300 ($n = 6$); each system was then placed in a 2.5 × 1.7 × 2.4 nm water box. In order to evaluate the entropic contribution to the formation of the H_2G adduct, MD simulations were also performed for the solutes; these consisted of one gemini guest inserted into two host molecules. This ensemble was put in a number of water molecules ranging from 685 ($n = 2$) to 700 ($n = 6$). The solute-solvent system thus obtained was finally placed in a 3.0 × 2.5 × 3.0 nm box. Consistent Valence Force Field (CVFF), combined with the CVFF flexible water potential, was used in all MD simulations;[60] furthermore Periodic Boundary Conditions (PBC) and Ewald summation, with a dielectric constant equal to 1, were applied. The calculations were run under NVT conditions at 298 K (using the thermostat of Berendsen with a decay constant of 1 ps) with a 1 fs time step. Electric neutrality condition was always maintained using Na^+ and Cl^- as counterions.

For the HG complexes simulations, an equilibration procedure which consists of 3000 minimization steps applied to solvent and solute was used then followed by 50 ns MD of the water molecules (while the solute was kept fixed); a further 250 ns MD simulation was carried out at the same temperature removing the constraint of the solute. During the last 100 ns, 10 structures were randomly sampled, optimized and used for successive first principle analysis.

As to the H_2G complexes, the same procedure was applied; however, in this case 6000 steps of minimizations and an overall simulation time of 600 ns were performed. Coordinates started to be sampled, for statistical analysis, after 400 ns.

DFT calculations were run for the HG complexes considering double positively charged systems. The solvation effects were modeled by means of Polarizable Continuum Model (PCM).[61] Tight optimizations criteria and an ultrafine grid were chosen to obtain relaxed geometries. The B97-D functional was considered in order to take account the dispersion effect; the extended 6-311+** basis set was employed.[62] Binding energies determined for the HG complexes are referred to the enthalpic contribution only and allow for the correction due to basis set superimposition error (BSSE).[63]

X-ray diffraction studies

Crystal structure determination of TAC4 and complexes 1, 2 and 3. Colorless crystals suitable for X-ray analysis were obtained by the vapor diffusion method, using the hanging drop technique, from a 8 μL drop, containing either 4 μL of **TAC4** (200 mM) or a **TAC4**/**BSC2** mixture (**BSC2** concentration 20 mM, molar ratios: 2 : 1, 8 : 1, 5 : 1) and 4 μL of the reservoir solution (PEG400 20–70%, imidazole buffer pH 7.1). Colorless crystals grew in one week at 5 °C.

Crystals were all of small dimensions and contained a large number of solvent molecules; consequently, to improve the intensity of the diffraction pattern, data collections were carried out using synchrotron radiation at the X-ray diffraction beamline of the Elettra Synchrotron, Trieste, Italy, employing the rotating-crystal method with the cryo-cooling technique. Owing to the components of the crystallization experiments, no further cryoprotection was required for diffraction experiments at 100 K.

Diffraction data of **1** and **3** were indexed and integrated using the MOSFLM,[64] while XDS package[65] was used for **TAC4** and **2**. Scaling was carried out with AIMLESS[66,67] in the case of **TAC4**, **1** and **2** and SCALA[64,65] for structure **3**. The structures of **1** and **2** were solved by direct methods using SIR2011.[68] The diffraction intensities of **3** show a symmetry belonging to the -31m Laue class. The systematic absences $l = 3n$ indicate the presence of screw axes 3_1 or 3_2. Several attempts to solve the structure in the $P3_112$ space group failed using direct methods. The solution was found in the $P3_1$ space group, using a merohedral twinning law of [0-1 0 -1 0 0 0 0 -1]. In the final refinement cycles with the detwinned hkl reflections (HKLF5 card) the Flack parameter suggested the inversion of the absolute configuration. Thus the inverted model coordinates were turned into the enantiomorphic $P3_2$ space group.

Non-hydrogen atoms at full occupancy, or with population equal to or higher than 0.6, were anisotropically refined (H atoms at the calculated positions) with bond length and angle restraints by full-matrix least-squares methods on F^2 using SHELXL-13.[69] Crystal data and refinement details are reported in Table S1.†

Treatment of the disorder

TAC4. In the crystal structure of **TAC4**, one chloride anion was found disordered over two positions, refined at 0.4/0.6 of partial occupancy; the chloride electron density was overlapped with a water molecule disordered over two positions which were refined with the same partial occupancy. Two water molecules were refined with partial population of 0.34 and 0.66.

1. In the crystal structure, one dimethylammonium group present at the calixarene upper rim was found disordered over two positions which were refined with 0.45/0.55 fractional occupancy. The chloride anion was found disordered over three positions, refined at 0.5/0.3/0.2 partial occupancy, and the half **BSC2** free guest disordered over two positions refined at half occupancy. The cell contains significantly disordered water molecules with partial occupancy that were not modeled but taken into account using the SQUEEZE/PLATON procedure.[70] The residual electron density of 114 electrons/cell found in the voids of **1** (corresponding to about 12% of the cell volume) was attributed to about 11 water molecules. The refinement using reflections modified by the SQUEEZE procedure succeeded and the *R*-factor was reduced from 16.5 to 11.9%.

2. The asymmetric unit consists of two independent complexes (**I** and **II**) depicted in Fig. S5.† The structure is affected by positional disorder which involves not only solvent molecules but also the **BSC2** guest for each of the complexes. In particular, in complex **I** two orientations were found for one sulphonate group. The two positions on the aromatic ring included in the calixarene cavity were refined with partial occupancy set to 0.8/0.2, respectively.

In the complex **II**, similar disorder over two positions of the sulphonate group on the guest aromatic ring inserted in the calixarene cavity was refined with the 0.9/0.1 partial occupancy. The sulphonate group present on the external aromatic ring of **BSC2** is affected by a rotational disorder and the two positions were refined at 0.9/0.1 of fractional occupancy. Analogously, 0.8/0.2 partial population refinement was used to deal with the disorder of the guest polymethylene bridge over two different conformations. The cell contains four disordered chloride anions refined at 0.85/0.15, 0.8/0.2, 0.75/0.25 and 0.6/0.4 of partial occupancy, respectively, 14 water molecules at full occupancy, 5 water molecules at 0.6, 0.5, 0.4, 0.2 of partial occupancy and two disordered over two positions refined at 0.75/0.25 and 0.8/0.2 of partial occupancy.

3. The asymmetric unit of the trimeric supramolecular aggregate contains a large amount of solvent molecules. 6 water molecules at full occupancy and 0.4/0.4/0.5/0.5/0.6/0.6/0.9 at partial occupancy could be identified or modeled in discrete positions as well as 3 chloride anions at full occupancy and 3 chloride anions disordered over two positions refined at 0.45/0.55, 0.5/0.5 and 0.4/0.6 of partial occupancy. Other significantly disordered solvent molecules with partial occupancy were not modeled but taken into account using the SQUEEZE[68] procedure. The residual electron density of 641 electrons/cell found in the voids of **3** (corresponding to about 17% of the cell volume) was attributed to about 64 water molecules. A refinement using reflections modified by the SQUEEZE procedure succeeded and the *R*-factor was reduced from 11.5 to 9.0%.

Acknowledgements

University of Catania and University of Trieste (FRA-2013 project) are gratefully acknowledged for partial support.

References

1 M. M. Conn and J. Rebek Jr, *Chem. Rev.*, 1997, **97**, 1647; F. Hof, S. L. Craig, C. Nuckolls and J. Rebek Jr, *Angew. Chem., Int. Ed.*, 2002, **41**, 1488.
2 P. Ballester, *Chem. Soc. Rev.*, 2010, **39**, 3810; L. Adriaenssensa and P. Ballester, *Chem. Soc. Rev.*, 2013, **42**, 3261.
3 M. D. Pluth and K. N. Raymond, *Chem. Soc. Rev.*, 2007, **36**, 161.
4 D. Garozzo, G. Gattuso, F. H. Kohnke, P. Malvagna, A. Notti, S. Occhipinti, S. Pappalardo and M. F. Parisi, *Tetrahedron Lett.*, 2002, **43**, 7663; G. Gattuso, A. Notti, A. Pappalardo, M. F. Parisi, I. Pisagatti, S. Pappalardo, D. Garozzo, A. Messina, Y. Cohen and S. Slovak, *J. Org. Chem.*, 2008, **73**, 7280.
5 M. Yamanaka, M. Kawaharada, Y. Nito, H. Takaya and K. Kobayashi, *J. Am. Chem. Soc.*, 2011, **133**, 16650; N. Nishimura, K. Yoza and K. Kobayashi, *J. Am. Chem. Soc.*, 2010, **132**, 777.
6 M. Yoshizawa, J. K. Klosterman and M. Fujita, *Angew. Chem., Int. Ed.*, 2009, **48**, 3418.
7 B. Breiner, J. K. Clegg and J. R. Nitschke, *Chem. Sci.*, 2011, **2**, 51.
8 A. Asadi, D. Ajami and J. Rebek Jr, *J. Am. Chem. Soc.*, 2011, **133**, 10682; J. Rebek Jr, *Acc. Chem. Res.*, 2009, **42**, 1660; G. Arena, A. Contino, E. Longo, C. Sgarlata, G. Spoto and V. Zito, *Chem. Commun.*, 2004, **16**, 1812.
9 M. Yoshizawa, M. Tamura and M. Fujita, *Science*, 2006, **312**, 251; L. S. Kaanumalle, C. L. D. Gibb, B. C. Gibb and V. Ramamurthy, *J. Am. Chem. Soc.*, 2005, **127**, 3674; S. Liu, H. Gan, A. T. Hermann, S. W. Rick and B. C. Gibb, *Nat. Chem.*, 2010, **2**, 847; M. D. Pluth, R. G. Bergman and K. N. Raymond, *Angew. Chem., Int. Ed.*, 2007, **46**, 8587.
10 M. Yoshizawa, T. Kuskawa, M. Fujita and K. J. Yamaguchi, *J. Am. Chem. Soc.*, 2000, **122**, 6311; D. Fiedler, R. G. Bergman and K. N. Raymond, *Angew. Chem., Int. Ed.*, 2006, **45**, 745; P. Mal, B. Breiner, K. Rissanen and J. R. Nitschke, *Science*, 2009, **324**, 1697.
11 H. Kumari, S. R. Klineb and J. L. Atwood, *Chem. Commun.*, 2012, **48**, 3599.
12 P. D. Beer and P. A. Gale, *Angew. Chem., Int. Ed.*, 2001, **40**, 486.
13 P. A. Gale, *Chem. Commun.*, 2011, **47**, 82; P. A. Gale and T. Gunnalaugsson, *Chem. Soc. Rev.*, 2010, **39**, 3595; J. W. Steed, *Chem. Soc. Rev.*, 2010, **39**, 3686; V. Amendola, L. Fabbrizzi and L. Mosca, *Chem. Soc. Rev.*, 2010, **39**, 3889.
14 *Anion Coordination Chemistry*, ed. K. Bowman-James, A. Bianchi and E. Garcia-Espana, Wiley-VCH, Weinheim,

2011; *Anion Receptor Chemistry, Monographs in Supramolecular Chemistry*, ed. J. L. Sessler, P. A. Gale and W. S. Cho, RSC Publishing, Cambridge, 2006.
15 C.-H. Tai, P. Burkhard, D. Gani, T. Jenn, C. Johnson and P. F. Cook, *Biochemistry*, 2001, **40**, 7446; B. T. Burlington and T. S. Widlanski, *J. Org. Chem.*, 2001, **66**, 7561.
16 P. F. Lito, J. P. S. Aniceto and C. M. Silva, *Water, Air, Soil Pollut.*, 2012, **223**, 6133; T. Cserhati, E. Forgacs and G. Oros, *Environ. Int.*, 2002, **28**, 337.
17 S. O. Kang, R. A. Begum and K. Bowman-James, *Angew. Chem., Int. Ed.*, 2006, **45**, 7882; P. A. Gale, J. R. Hiscock, C. Z. Jie, M. B. Hursthouse and M. E. Light, *Chem. Sci.*, 2010, **1**, 215; K. A. Schug and W. Lindner, *Chem. Rev.*, 2005, **105**, 67; P. Mateus, N. Bernier and R. Delgado, *Coord. Chem. Rev.*, 2010, **254**, 1726.
18 M. Arunachalam and P. Ghosh, *Chem. Commun.*, 2011, **47**, 8477.
19 M. D. Lankshear and P. D. Beer, *Acc. Chem. Res.*, 2007, **40**, 657; R. Vilar, *Angew. Chem., Int. Ed.*, 2003, **42**, 1460.
20 S. Kubik, *Chem. Soc. Rev.*, 2010, **39**, 3648.
21 G. O. Oshovsky, D. N. Reinhoudt and W. Verboom, *Angew. Chem., Int. Ed.*, 2007, **46**, 2366; F. Corbellini, A. Mulder, A. Sartori, M. J. W. Ludden, A. Casnati, R. Ungaro, J. Huskens, M. Crego-Calama and D. N. Reinhoudt, *J. Am. Chem. Soc.*, 2004, **126**, 17050.
22 F. Sansone and A. Casnati, *Chem. Soc. Rev.*, 2013, **42**, 4623.
23 S. M. Biros and J. Rebek Jr, *Chem. Soc. Rev.*, 2007, **36**, 93.
24 Z. Laughreya and B. C. Gibb, *Chem. Soc. Rev.*, 2011, **40**, 363; C. L. D. Gibb and B. C. Gibb, *Tetrahedron*, 2009, **65**, 7240.
25 O. V. Surov, M. A. Krestianinov and M. I. Voronova, *Spectrochim. Acta, Part A*, 2015, **134**, 121.
26 F. Billes, I. Mohammed-Ziegler and H. Mikosch, *J. Mol. Model.*, 2012, **18**, 3627.
27 C. Sgarlata, C. Bonaccorso, F. G. Gulino, V. Zito, G. Arena and D. Sciotto, *New J. Chem.*, 2009, **33**, 991; C. Sgarlata, C. Bonaccorso, F. G. Gulino, V. Zito, G. Arena and D. Sciotto, *Tetrahedron Lett.*, 2009, **50**, 1610.
28 C. Bonaccorso, A. Ciadamidaro, V. Zito, C. Sgarlata, D. Sciotto and G. Arena, *Thermochim. Acta*, 2012, **530**, 107.
29 C. Bonaccorso, A. Ciadamidaro, C. Sgarlata, D. Sciotto and G. Arena, *Chem. Commun.*, 2010, **46**, 7139.
30 C. Bonaccorso, C. Sgarlata, G. Grasso, V. Zito, D. Sciotto and G. Arena, *Chem. Commun.*, 2011, **47**, 6117.
31 C. Sgarlata, G. Arena, D. Sciotto and C. Bonaccorso, *Supramol. Chem.*, 2013, **25**, 696.
32 F. P. Schmidtchen, *Chem. Soc. Rev.*, 2010, **39**, 3916.
33 H.-X. Zhao, D.-S. Guo and Y. Liu, *J. Phys. Chem. B*, 2013, **117**, 1978.
34 E. A. Meyer, R. K. Castellano and F. Diederich, *Angew. Chem., Int. Ed.*, 2003, **42**, 1210.
35 M. Nishio, *Tetrahedron*, 2005, **61**, 6923.
36 E. Grunwald and C. Steel, *J. Am. Chem. Soc.*, 1995, **117**, 5687; K. N. Houk, A. G. Leach, S. P. Kim and X. Zhang, *Angew. Chem., Int. Ed.*, 2003, **42**, 4872; G. Arena, R. Calì, E. Rizzarelli and S. Sammartano, *Thermochim. Acta*, 1976, **17**, 155.
37 D. H. Leung, R. G. Bergman and K. N. Raymond, *J. Am. Chem. Soc.*, 2008, **130**, 2798.
38 H. Gan, C. J. Benjamin and B. C. Gibb, *J. Am. Chem. Soc.*, 2011, **133**, 4770.
39 E. L. Eliel, in *Steric Effects in Organic Chemistry*, ed. M. S. Newman, Wiley, New York, 1956, p. 138.
40 R. Foster, in *Organic Charge Transfer Complexes*, Academic Press, London, 1969, p. 199.
41 G. Adamová, J. N. Canongia Lopes, L. P. N. Rebelo, L. M. N. B. Santos, K. R. Seddon and K. Shimizu, *Phys. Chem. Chem. Phys.*, 2014, **16**, 4033.
42 G. Bai, M. Nichifor, A. Lopes and M. Bastos, *J. Phys. Chem. B*, 2005, **109**, 518; M. Nichifor, M. Bastos, S. Lopes and A. Lopes, *J. Phys. Chem. B*, 2008, **112**, 15554.
43 F. Tao and S. L. Bernasek, *Chem. Rev.*, 2007, **107**, 1408.
44 J. C. S. Costa, M. Fulem, B. Schroder, J. A. P. Coutinho, M. J. S. Monte and L. M. N. B. F. Santos, *J. Chem. Thermodyn.*, 2012, **54**, 171.
45 R. T. Morrison and R. N. Boyd, in *Organic Chemistry*, Prentice Hall, Englewood Cliffs, 6th edn, 1992, pp. 713–718.
46 C. Sgarlata, V. Zito and G. Arena, *Anal. Bioanal. Chem.*, 2013, **405**, 1085.
47 N. A. Demarse, C. F. Quinn, D. L. Eggett, D. J. Russell and L. D. Hansen, *Anal. Biochem.*, 2011, **417**, 247.
48 I. Wadso and L. Wadso, *J. Therm. Anal. Calorim.*, 2005, **82**, 553.
49 J. Kang and J. Rebek Jr, *Nature*, 1996, **382**, 239.
50 C. Sgarlata, J. S. Mugridge, M. D. Pluth, B. E. F. Tiedemann, V. Zito, G. Arena and K. N. Raymond, *J. Am. Chem. Soc.*, 2010, **132**, 1005.
51 A. R. Albunia, C. Gaeta, P. Neri, A. Grassi and G. Milano, *J. Phys. Chem. B*, 2006, **110**, 19207.
52 F. Corbellini, L. Di Costanzo, M. Crego-Calama, S. Geremia and D. N. Reinhoudt, *J. Am. Chem. Soc.*, 2003, **125**, 9946; E. Botana, K. Nattinen, P. Prados, K. Rissanen and J. de Mendoza, *Org. Lett.*, 2004, **6**, 1091; F. Corbellini, F. W. B. van Leeuwen, H. Beijleveld, H. Kooijman, A. L. Spek, W. Verboom, M. Crego-Calama and D. N. Reinhoudt, *New J. Chem.*, 2005, **29**, 243; L. Grubert, H. Hennig and W. Abraham, *Tetrahedron*, 2009, **65**, 5936; L.-L. Liu, H.-X. Li, L.-M. Wan, Z.-G. Ren, H.-F. Wang and J.-P. Lang, *Chem. Commun.*, 2011, **47**, 11146; L.-L. Liu, Z.-G. Ren, L.-M. Wan, H.-Y. Ding and J.-P. Lang, *CrystEngComm*, 2011, **13**, 5718.
53 J. L. Atwood, G. W. Orr, S. G. Bott and K. D. Robinson, *Angew. Chem., Int. Ed.*, 1993, **32**, 1093; D. J. E. Spencer, B. J. Johnson, B. J. Johnson and W. B. Tolman, *Org. Lett.*, 2002, **4**, 1391; J. Zhang, D. S. Guo, L. H. Wang, Z. Wang and Y. Liu, *Soft Matter*, 2011, **7**, 1756; E. K. Bullough, C. A. Kilner, M. A. Little and C. E. Willans, *Org. Biomol. Chem.*, 2012, **10**, 2824.
54 F. Billes and I. Mohammed-Ziegler, *Supramol. Chem.*, 2002, **14**, 451.
55 J. L. Atwood, L. J. Barbour, M. J. Hardie and C. L. Raston, *Coord. Chem. Rev.*, 2001, **222**, 3; A. W. Coleman, S. G. Bott, S. D. Morley, C. M. Means, K. D. Robinson, H.-M. Zhang and J. L. Atwood, *Angew. Chem., Int. Ed. Engl.*, 1988, **27**, 1361.

56 H. P. G. Thompson and G. M. Day, *Chem. Sci.*, 2014, **5**, 3173.
57 C. D. Gutsche and K. C. Nam, *J. Am. Chem. Soc.*, 1988, **110**, 6153.
58 D. R. Bundle and B. W. Sigurskjold, *Methods Enzymol.*, 1994, **247**, 288; L. D. Hansen, G. W. Fellingham and D. J. Russell, *Anal. Biochem.*, 2011, **409**, 220.
59 P. Gans, A. Sabatini and A. Vacca, *J. Solution Chem.*, 2008, **37**, 467.
60 P. Dauber-Osguthorpe, V. A. Roberts, D. J. Osguthorpe, J. Wolff, M. Genest and A. T. Hagler, *Proteins: Struct., Funct., Genet.*, 1988, **4**, 31; K. F. Lau, H. E. Alper, T. S. Thacher and T. R. Stouch, *J. Phys. Chem.*, 1994, **98**, 8785.
61 A. Klamt and G. J. Schüürmann, *J. Chem. Soc., Perkin Trans. 2*, 1993, **5**, 799; M. Cossi, N. Rega, G. Scalmani and V. Barone, *J. Comput. Chem.*, 2003, **24**, 669.
62 A. D. McLean and G. S. Chandler, *J. Chem. Phys.*, 1980, **72**, 5639; R. Krishnan, J. S. Binkley, R. Seeger and J. A. Pople, *J. Chem. Phys.*, 1980, **72**, 650; R. C. Binning Jr and L. A. Curtiss, *J. Comput. Chem.*, 1990, **11**, 1206.
63 S. F. Boys and F. Bernardi, *Mol. Phys.*, 1970, **19**, 553; S. Simon, M. Duran and J. J. Dannenberg, *J. Chem. Phys.*, 1996, **105**, 11024.
64 G. G. Battye, L. Kontogiannis, O. Johnson, H. R. Powell and A. G. W. Leslie, *Acta Crystallogr., Sect. D: Biol. Crystallogr.*, 2011, **67**, 271.
65 W. Kabsch, *Acta Crystallogr., Sect. D: Biol. Crystallogr.*, 2010, **66**, 125.
66 P. R. Evans, *Acta Crystallogr., Sect. D: Biol. Crystallogr.*, 2006, **62**, 72.
67 M. D. Winn, C. C. Ballard, K. D. Cowtan, E. J. Dodson, P. Emsley, P. R. Evans, R. M. Keegan, E. B. Krissinel, A. G. W. Leslie, A. McCoy, S. J. McNicholas, G. N. Murshudov, N. Pannu, E. A. Potterton, H. R. Powell, R. J. Read, A. Vagin and K. S. Wilson, *Acta Crystallogr., Sect. D: Biol. Crystallogr.*, 2011, **67**, 235.
68 M. C. Burla, R. Caliandro, M. Camalli, B. Carrozzini, G. L. Cascarano, L. De Caro, C. Giacovazzo, G. Polidori, D. Siliqi and R. Spagna, *J. Appl. Crystallogr.*, 2007, **40**, 609.
69 G. M. Sheldrick, *Acta Crystallogr., Sect. A: Found. Crystallogr.*, 2008, **64**, 112.
70 P. van der Sluis and A. L. Spek, *Acta Crystallogr., Sect. A: Found. Crystallogr.*, 1990, **46**, 194.